IOP Publishing Journal of Physics: Condensed Matter
J. Phys.: Condens. Matter **32** (2020) 255402 (13pp) https://doi.org/10.1088/1361-648X/ab7a4a

Magneto-elastic properties of a spin crossover membrane deposited on a deformable substrate

K Affes[1,2], A Slimani[1,3,4], Y Singh[2], A Maalej[1] and K Boukheddaden[2]

[1] Laboratoire des Matériaux Multifonctionnels et Applications, Université de Sfax, Faculté des Sciences de Sfax, Route de la Soukra km 3.5, 3000, Sfax, Tunisia
[2] GEMaC, CNRS—Université de Versailles Saint Quentin en Yvelines, 45 Avenue des Etats Unis, F-78035 Versailles Cedex, France
[3] Sciences and Engineering Department, Sorbonne University Abu Dhabi, Al Reem island, Abu Dhabi, PO Box 38044, United Arab Emirates

E-mail: ahmed.slimani@fss.rnu.tn and kamel.boukheddaden@uvsq.fr

Received 1 January 2020, revised 27 January 2020
Accepted for publication 26 February 2020
Published 27 March 2020

Abstract

Spin-crossover (SCO) solids have been studied for several years due to their fascinating physical properties and their potential applications as optical switches and reversible high-density memories for information storage. Through this article, we will examine in details the effects of substrate's lattice parameters, on a deformable spin crossover membrane, simulated using an electro-elastic model taking into account the volume change at the transition. The molecules of the membrane can be either in the low spin state (LS) or the high spin state (HS), while those of the substrate are electronically neutral. Magnetic properties of the SCO membrane and the pressure distribution as a function of the lattice parameter of the substrate have been investigated. We demonstrated that the thermally induced first-order spin transition is significantly affected by the structural properties of the substrate, where a rise in the lattice parameter of the latter lowers the transition temperature and reduces the width of the thermal hysteresis loop. The investigations on the spatiotemporal aspects of the spin transition in the membrane demonstrates that the nucleation and growth processes are sensitive to the structural properties of the elastic misfit between the substrate and the SCO membrane.

Keywords: spin-crossover, Monte-Carlo, phase transition, bistability, membrane–substrate

Supplementary material for this article is available online

(Some figures may appear in colour only in the online journal)

1. Introduction

SCO compounds [1] are molecular solids able to switch between two spin states, namely, the low spin state (LS) and the high spin state (HS), having different magnetic, mechanical, optical and vibrational properties. The switching between the LS and HS states can be realized by applying external stimuli such as pressure [2, 3], temperature [4], magnetic field [5] and electric field [6], etc.

The spin-crossover SCO compounds, in particular those with octahedral symmetry where the metal ion is coordinated to nitrogen atoms, are among the most studied molecular switchable materials. The case of Fe(II)-based SCO materials, with $3d^6$ configuration, is the most common in literature, with a total spin equal to $S = 2$ and $S = 0$, in HS and LS states, respectively. In these ferrous SCO compounds, the five d-orbitals of iron(II) are then split into three t_{2g} and two e_g orbitals. According to the strength of the ligand field, $\Delta = E\left(t_{2g}\right) - E(e_g)$, the metal ion can be in the LS (resp. HS)

[4] Author to whom any correspondence should be addressed.

state when Δ is much stronger (weaker) than the electrons pairing energy. The resulting spin state then emerges from the balance between the energy of the orbital, needed to occupy all of the 3d levels in order to maximize the spin state and the average energy of the Coulomb repulsion of the d-electrons. In the solid state, the thermal properties of SCO materials gives rise to a rich variety of behaviors, ranging from (i) a simple continuous gradual spin-transition corresponding to a Boltzmann population of two degenerate states to (ii) sharp first-order transitions, including (iii) incomplete transitions, with the presence of a nonzero residual HS fraction at low-temperature and (iv) two-step or multi-step spin transitions, characterized by the presence of a macroscopic intermediate state in the course of the transition between the LS and the HS states [7, 8].

From the chemistry point of view, all these behaviors are obtained by changing the nature, the size or the mode of the ligand or the anions (BF_4, PF_6, ...) which affects the crystal packing, resulting in important changes at the macroscopic scale. The spin transition of the metal ion, which redistributes the electrons occupancy between t_{2g} and e_g orbitals is accompanied by a huge relative change of the molecular volume by about 30%, while the volume change of the unit cell is only 3%–5% [9, 10]. This difference is due to the existence of a structural reorganization at the molecular level, among which the reorientation and/or the distortion of the ligands. This local volume change deploys far from the sources as a shock wave which reflects at the surface of the material causing an image pressure [11–14], which results in long-range stresses acting on the other molecules of the lattice. The strength of this mechanism of interaction between the SCO molecules is enhanced by the constructive interferences taking place between the strain fields caused by the local volume changes of several molecules located at different positions in the material; thus inducing collective phenomena which are at the origin of the cooperativity of SCO solids.

Due to the various changes of the physical properties accompanying the spin transition, the SCO systems were characterized experimentally by several techniques, among which, magnetic [15–17], optical [18] and structural [19] techniques are the most used ones. Thus, for example, squid (superconducting quantum interference device) measurements, Mössbauer spectroscopy, optical microscopy (OM), x-ray diffraction, calorimetry [20–39], have been intensively used to understand the thermo- and photo-induced properties of SCO materials. This abundance in the change of physical properties on the same compound concomitant with the spin transition makes these systems very promising for technological applications, as electronic and memory devices [40–43], sensors of (i) temperature when they are photo- or electro-luminescent [44], (ii) pressure [2, 45], (iii) gases [46], as well as (iv) switches of light emission in electroluminescent or plasmonic devices [47, 48], in addition to their very recent applications in spintronics [49–51].

From the fundamental point of view, it is well admitted that the intermolecular interactions play a crucial role in the emerging thermodynamic properties of SCO at the macroscopic scale. According to their strengths, they may lead to different behaviors, going from gradual spin transition [52] to first-order phase transition [53] with thermal hysteresis in strongly cooperative samples. However, several unconventional behaviors of SCO materials could be found in literature. One can mention, for example, the case of two- or multi-steps transitions which have been reported in several systems, and usually attributed to the existence of competing interactions. Typical examples are found in binuclear systems [54, 55], or in mononuclear systems exhibiting a structural order–disorder phase transition coupled to the spin transition [54, 56–59].

From the theoretical point of view, different models were introduced to reproduce the thermodynamic properties of SCO solids, such as the Ising-like model [56, 60, 61], atom phonon model [62, 63] and recently elastic models [64–85], which are the most realistic ones.

The case of the relationship between the SCO membrane or thin film attached to a substrate is challenging to clarify from the theoretical point of view. Indeed, the switchable and distortable membrane deposited on a substrate displays a variety of complex phenomena due to the change of its elastic properties along its spin transition (lattice contraction or expansion) which produces a strain in the substrate, which in turn induces a stress on the SCO thin film, whose features depend on the difference of elastic moduli and lattice parameter misfit between the two sub-lattices.

In this paper, we consider from a theoretical point of view an SCO membrane deposited on a substrate modeled through a microscopic electro-elastic model [69–72]. The later has shown its performance in the analysis of the thermal spin transition of SCO systems in succeeding to correctly describe the spatiotemporal aspects of SCO single crystals [70, 71] and nanoparticles [86–90] along their thermally- and light-induced spin transitions. The additional insight gained through this study will be a fundamental step toward the explanation of the structural and mechanical relationship between the membrane and the substrate. This study is based on Monte Carlo (MC) simulations of a 2D lattice, conducted on spin and positions degrees of freedom. The lattice parameters of SCO membrane and the substrate were chosen so as to have a structurally hybrid system with two different lattice parameters.

The manuscript is organized as follows: in section 2, we present the electro-elastic model, and describe the simulation procedure. Section 3 is devoted to study the mechanical relaxation of the total lattice as well as the analysis of the thermo-induced spin transition of the SCO membrane and the spatiotemporal aspects are discussed. In section 4, we conclude the paper and outline the possible developments of the present work.

2. Hamiltonian

We investigated a distortable 2D rectangular lattice with a fixed topology and open boundary conditions. The system is composed of a 10 layers thickness SCO membrane attached to a substrate having 20 layers thickness. The membrane and the substrate have the same length, composed of 40 atomic sites (see the schematic view figure 1a). According to figure 1a, the present model considers the study of the vertical cross-section of the true corresponding 3D membrane–substrate

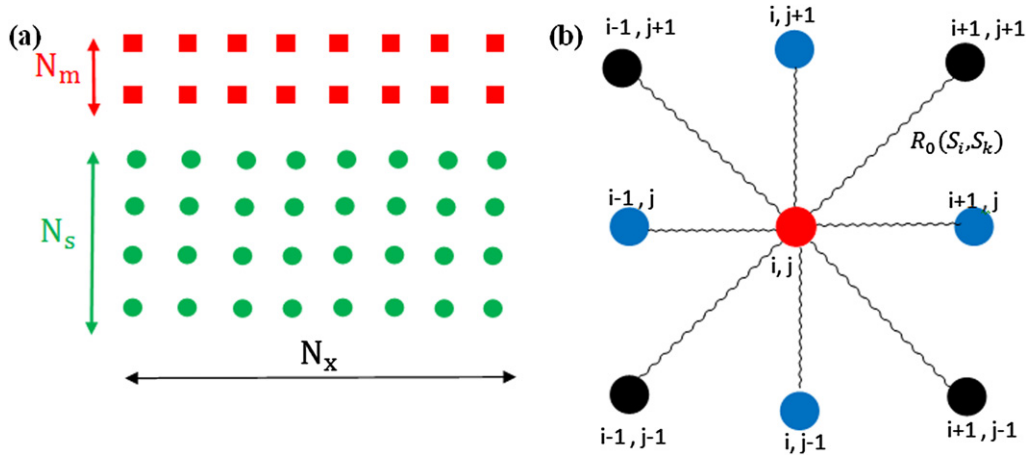

Figure 1. (a) Schematic view of the SCO membrane deposited on a substrate. Green dots and red squares are respectively the substrate and the membrane atoms. N_{m} and N_{s} are the membrane and substrate thicknesses, respectively, and $N_{\mathrm{x}}$is the system's length. (b) Configuration of the elastic interactions in this 2D square model.

system, whose investigations using elastic modeling is currently out of reach.

Each node of SCO membrane can have two electronic states, namely HS and LS, represented by an associated fictitious spin S_i, whose values are $S_i = -1$ and $S_i = +1$ for LS and HS states, respectively.

The substrate does not have any electronic contribution, while the sites of the whole lattice (membrane + substrate) are allowed to move only inside the plane. The electro-elastic Hamiltonian writes as follows:

$$H = H_{\mathrm{s}} + H_{\mathrm{m}} + H_{\mathrm{ms}} \tag{1}$$

where $H_{\mathrm{s}}, H_{\mathrm{m}}$ and $H_{\mathrm{m-s}}$ stand for the Hamiltonian contributions of the substrate, the membrane and the membrane–substrate interface, respectively. The expressions of the different Hamiltonians are given as follows:

$$H_{\mathrm{m}} = \sum_{i\in\mathrm{mem}} \frac{(\Delta - k_{\mathrm{B}}T\ \ln\ g)\,S_i}{2} + \sum_{i,j\in\mathrm{mem}}^{\mathrm{nn}} A_{ij}\left[r_{ij} - R_0\left(S_i,S_j\right)\right]^2 + \sum_{i,k\in\mathrm{mem}}^{\mathrm{nnn}} B_{ik}\left[r_{ik} - R_0'\left(S_i,S_k\right)\right]^2, \tag{2}$$

$$H_{\mathrm{s}} = \sum_{i,j\in\mathrm{sub}}^{\mathrm{nn}} A_{\mathrm{sub}}\left[r_{ij} - R_{\mathrm{sub}}\right]^2 + \sum_{i,k\in\mathrm{sub}}^{\mathrm{nnn}} B_{\mathrm{sub}}\left[r_{ik} - R'_{\mathrm{sub}}\right]^2, \tag{3}$$

$$H_{\mathrm{m-s}} = \sum_{i\in\mathrm{mem}} \frac{(\Delta - k_{\mathrm{B}}T\ \ln\ g)\,S_i}{2} + \sum_{i,j\in\mathrm{mem,sub}}^{\mathrm{nn}} A_{ij}\left[r_{ij} - R_{\mathrm{mem-sub}}\left(S_i,S_j\right)\right]^2 + \sum_{i,k\in\mathrm{mem,sub}}^{\mathrm{nnn}} B_{ik}\left[r_{ik} - R'_{\mathrm{mem-sub}}\left(S_i,S_k\right)\right]^2, \tag{4}$$

The Hamiltonian of the SCO membrane, given by equation (2), contains the entropic effects ($k_{\mathrm{B}}T\ \ln\ g$) arising from the degeneracy ratio, g, between the HS and LS states and the energetic contribution of the ligand fields in the HS and LS states, such as $\Delta = E_{\mathrm{HS}} - E_{\mathrm{LS}}$ corresponding to the energy difference between the HS and LS states at 0 K.

The second and third terms in equation (2) are the elastic contributions of the lattice, where the quantity $R_0\left(S_i,S_j\right)$ and $R_0'\left(S_i,S_k\right)$ are the nearest-neighbors (nn) and next-nearest neighbors (nnn) equilibrium distances, which depend on the spin states of the connected bonds. The equilibrium bond lengths in the SCO membrane are defined as follow: $R_0\left(-1,-1\right) = R_0^{\mathrm{LL}}$, $R_0\left(+1,+1\right) = R_0^{\mathrm{HH}}$ and $R_0\left(+1,-1\right) = R_0\left(-1,+1\right) = R_0^{\mathrm{HL}}$ for the LS–LS, HS–HS and HS–LS sites configurations, respectively. For simplicity, we consider, $R_0^{\mathrm{HL}} = \frac{1}{2}(R_0^{\mathrm{HH}} + R_0^{\mathrm{LL}})$. The general expression of the nn distance writes:

$$R_0\left(S_i,S_j\right) = R_0^{\mathrm{HL}} + \frac{\delta R}{4}\left(S_i + S_j\right), \tag{5}$$

where $\delta R = R_0^{\mathrm{HH}} - R_0^{\mathrm{LL}}$is the lattice misfit between the LS and HS phases. In equations (2)–(4), r_{ij} and r_{ik} are respectively the instantaneous distances between two nn and nnn sites. A_{ij} (resp. A_{sub}) and B_{ik} (resp. B_{sub}) are respectively the corresponding local bond stiffness between nn and nnn sites in the membrane (resp. the substrate). The elastic constant in the membrane writes as:

$$\begin{aligned} A_{ij}\left(r_{ij}\right) &= A_0 + A_1\left(r_{ij} - R_0^{HH}\right)^2 \quad \text{and} \\ B_{ik}\left(r_{ik}\right) &= B_0 + B_1\left(r_{ik} - \sqrt{2}R_0^{\mathrm{HH}}\right)^2 \end{aligned} \tag{6}$$

A_0 (resp. B_0) and A_1 (resp. B_1) are the harmonic and the anharmonic contributions to the elastic interaction energy between nn (resp. nnn) neighbors. We should mention that the anharmonicity is introduced here in order to fulfill the experimental observations indicating that the HS state has a lower bulk modulus than the LS state [91, 92].

In contrast, we have considered purely harmonic elastic interactions for the substrate lattice (equation (3)), with elastic constants, A_{sub} and B_{sub} and equilibrium lattice parameter, R_{sub}. Along the simulations developed here, different values of R_{sub} will be considered.

Table 1. Model parameter values used in MC the simulations.

Model parameters	Values
Degeneracy ratio g	150 [56, 60, 94]
Ligand field energy Δ(K)	600
Transition temperature $T_{eq} = \frac{\Delta}{k_B \ln g}$ (K)	120
Enthalpy change ΔH (k J mol^{-1})	5
Entropy change ΔS (J K^{-1} mol^{-1})	41.63
nn distance of HS state $R_0(+1,+1)$ (nm)	1.2
nn distance of LS state $R_0(-1,-1)$ (nm)	1
nn distance of HL state $R_0(+1,-1)$ (nm)	1.1
LS nnn distance $\sqrt{2}R_0(-1,-1)$ (nm)	1.4
HS nnn distance $\sqrt{2}R_0(+1,+1)$ (nm)	1.7
nn elastic constants A_0 (K nm^{-2})	3×10^4
nnn elastic constants B$_0$ (K nm^{-2})	$0, 3A_0$
Anharmonic nn elastic constant A_1 (K nm^{-2})	$10A_0$
Anharmonic nnn elastic constant B$_1$ (K nm^{-2})	$10B_0$

The Hamiltonian (4) describes the energetic contribution of the atoms located at the interface membrane–substrate, where the elastic interactions for the nn and nnn are, A_{ij} and B_{ik}, respectively.

The equilibrium bond lengths, $R_{\text{mem-sub}}$, at the interface membrane–substrate depend on the membrane spin state, S_i, as follows, $R_{\text{mem-sub}} = \frac{R_{\text{sub}}+R_0(S_i,S_j)}{2}$, which leads to $R_{\text{mem-sub}} = \frac{R_{\text{sub}}+R_0^{\text{HH}}}{2}$ (resp. $R_{\text{mem-sub}} = \frac{R_{\text{sub}}+R_0^{\text{LL}}}{2}$) for a substrate site connected to an HS (resp. LS) membrane site.

The model's parameter values used along the paper are summarized in table 1. We should mention that the values of the ligand field energy, Δ, and the effective degeneracy, g, are derived from experimental data of calorimetry, in which typical enthalpy variation ΔH at the spin transition are ranged between 5 and 20 kJ mol^{-1} with entropy ΔS in the range 35–80 J K^{-1} mol^{-1} [93]. These two quantities connect to Δ and g through the relations, $\Delta H = \Delta N_A$ and $\Delta S = R \ln g$, where N_A is the Avogadro number and R is the perfect gas constant.

It is worth mentioning that the Fe–ligand distance changes from 2.2 Å in HS to 2 Å in LS in the spin transition of Fe(II)-based SCO compounds. However, the lattice parameter is around 1 nm in SCO solids and its relative change upon spin transition from LS to HS is of approximately 5% or even more, depending on the structure, and the nature of the molecular stacking (pi–pi interactions, H–H bonding etc). However, the relevant quantity in the present model is the misfit elastic energy, evaluated as $\sim \frac{1}{2}(A+2B)(R_0^{\text{HH}} - R_0^{\text{LL}})^2$. So, the elastic constants (A and B) and the lattice parameter misfit, $\delta R = R_0^{\text{HH}} - R_0^{\text{LL}}$ play on the same way. So, the choice of a large lattice spacing mismatch allows a better visibility of the elastic effects by enhancing the lattice distortions. According to the chosen values of elastic constants, $A \sim 30.000$ K nm^{-2}, a bulk modulus value, $E \simeq 3$ GPa is estimated in fair agreement with available experimental data. At last, decreasing the lattice spacing misfit at the transition and enhancing the elastic constants, will lead qualitatively to the same results.

It can be mentioned that the present Hamiltonian generates long- and short-range interactions [70, 89, 95] between the spin states. The long-range interactions are due to the macroscopic volume change at the transition and the short-range interactions originate from fictious spin-spin 'exchange' interactions via lattice distortions. The technical aspects of the simulations, already presented in previous papers [96], are summarized in section I of the supplemental material.

3. Results and discussion

In the present study, we considered two different equilibrium lattice parameters for the SCO membrane and the substrate, namely R_{mem} and R_{sub}, respectively. The simulation strategy is as follow: initially at 0 K, we build the system (membrane + substrate) with the same lattice parameter that of the substrate, i.e. $R_{\text{mem}} = R_{\text{sub}}$. Then, we relax mechanically the whole system in order to satisfy the structural equilibrium of each component, since the equilibrium lattice parameters R_{mem} and R_{sub} are different. Finally, we investigate the thermo-induced spin transition.

It is worth to mention that, the present 2D lattice is an over simplified description that has the merit of being numerically tractable although it masks several 3D effects. From the point of view of simulations, the study of elastic 3D systems was conducted in a prior work in order to study the crumpling effects created by the volume change during the spin transition [97] and more recently intensive simulations on cubic and spherical shaped lattices have been conducted by Enachescu *et al* [98].

3.1. 0 K mechanical relaxation of the membrane–substrate lattice

Initially, we fixed the equilibrium lattice parameter of the SCO membrane as 1, 0 nm ($= R_0^{\text{LL}}$) and we varied that of the substrate in the range 0.9–1.3 nm. Then, we mechanically relax the whole system (membrane + substrate) using 100 000 MCS. The relaxation process is monitored by the 'stationary' character of the total elastic energy. Figures S1(a) and 2(a) show the time dependence of the average membrane, $\langle r^{\text{mem}} \rangle$, and substrate, $\langle r^{\text{sub}} \rangle$, bond lengths as functions of, R_{sub}. The substrate's lattice parameter significantly influences the post-relaxation lattice parameters of the membrane, $\langle r_\infty^{\text{mem}} \rangle$, and the substrate, $\langle r_\infty^{\text{sub}} \rangle$, where $\langle r_\infty \rangle$ denotes the lattice parameter at the mechanical equilibrium (i.e. at infinite time).

At the beginning of the relaxation process, $\langle r^{\text{sub}} \rangle$ (figure 2(a)) reveals an abrupt and non monotonous behavior. This fact is attributed to the fast mechanical relaxation of the membrane. More the misfit between the lattice parameters of the membrane and the substrate is important, more the retroaction of the substrate is significant, as we can easily notice at the beginning of the relaxation process of the substrate on figure 2(a).

We have investigated as well the spatial dependence of the local pressure, P_i, given by

$$P_i = -\sum_j A_{ij}(r_{ij})(r_{ij} - R_{\text{eq}}) - \sum_k B_{ik}(r_{ik})\left(r_{ik} - \sqrt{2}R_{\text{eq}}\right) \quad (7)$$

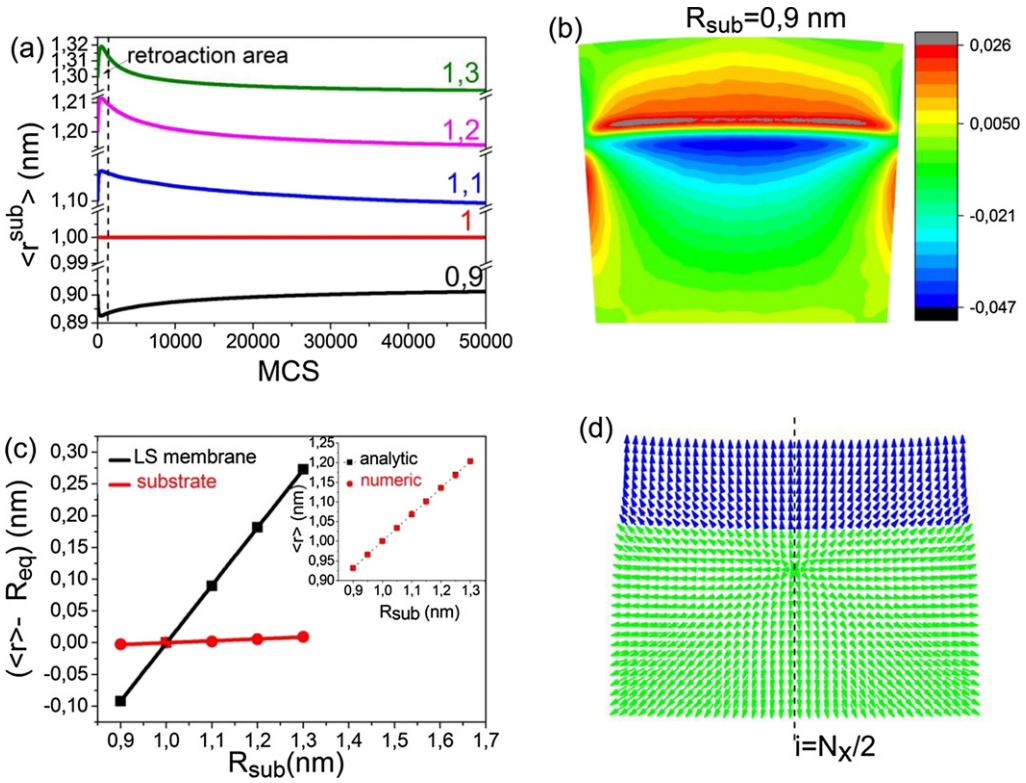

Figure 2. (a) 0 K time dependences of the average lattice parameters of the membrane $\langle r^{\mathrm{mem}}\rangle$ during the mechanical relaxation for different substrate equilibrium lattice parameters, R_{sub}, ranging in the interval 0.9–1.3nm. (b) Distribution of the local pressure at 0 K for $R_{\mathrm{sub}} = 0.9$nm. (c) $\langle r\rangle - R_{\mathrm{eq}}$ at mechanical equilibrium of the membrane and the substrate as a function of substrate's lattice parameter. Inset: comparison between the analytical and numerical results for the average lattice parameter of the whole system. (d) Spatial map of the displacement fields corresponding to the mechanical equilibrium for the initial value $R_{\mathrm{sub}} = 1$nm. The reference of displacement field is the initial state where $R_{\mathrm{mem}} = R_{\mathrm{sub}} = R_0^{\mathrm{LL}} = 1$ nm. The dashed line corresponds to $i = \frac{N_{\mathrm{x}}}{2}$. The horizontal size is $N_{\mathrm{x}} = 40$.

where the indexes j and k run over the nn and nnn of the site i, respectively.

The distribution of the local pressure over the relaxed membrane, at 0 K, are reported in the figures 2(b) and S1(b) for $R_{\mathrm{sub}} = 0.9$ nm and 1.3 nm, respectively. For lower substrate's lattice parameter, the SCO membrane undergoes a positive pressure that prevents the volume expansion and thus the LS $\rightarrow$ HS transition. However, the situation is reversed with higher R_{sub}. The pressure is mainly localized on the interface region which appears more pinched, leading to the rise of pressure. Such a constrained situation promotes the LS state, where the hysteresis loop was narrowed for substrate's lattice parameter smaller than that of the SCO membrane.

Figure 2(c) reports the difference between the average relaxed bond lengths $\langle r\rangle$ and the equilibrium one, R_{eq}, for the membrane and the substrate as a function of the substrate's lattice parameter. Indeed, the substrate remains unaffected by this change due to its large size ($N_{\mathrm{s}} = 20$). The membrane's relaxed lattice parameter follows a linear trend and increases with R_{sub}. The rate of this expansion clearly depends on the coupling at the interface between the two subsystems and on their relative rigidities.

Now, we focus on the stress generated by the mechanical relaxation, which has been shown to be important in the experiments [90]. The elastic stress was evaluated at 0 K. We estimated the displacement field $\vec{u}(i, j)$ associated with the lattice site (i, j) defined as: $\vec{u}(i, j) = \vec{r}(i, j) - \vec{r}_0(i, j)$, where $\vec{r}_0(i, j)$ is the initial atomic position of the sites (i, j) and $\vec{r}(i, j)$ is the position at mechanical equilibrium. In the present data analysis, we used the positions of the perfect LS lattice as a reference state: $\vec{r}_0(i, j) = \left(i \times R_0^{\mathrm{LL}}, j \times R_0^{\mathrm{LL}}\right)$.

In figures S2(c) and 2(d), the spatial map of the displacement field $\vec{u}(i, j)$ of the system at 0 K shows a global contraction of the membrane for $R_{\mathrm{sub}} = 1.1$ nm. In particular, the nodes situated at the interface membrane/substrate, are characterized by a large displacement, while the sites at the edges and corners of the membrane are quasi-static. Indeed, in the first case, the membrane shrinks until it reaches the mechanical equilibrium, $R_{\mathrm{mem}} = R_0^{\mathrm{LL}} = 1$ nm. However, in the other case ($R_{\mathrm{sub}} \neq 1$ nm), an important expansion appears especially in the substrate until it reaches the final equilibrium state ($R_{\mathrm{sub}} = 1.1$ nm). The analysis of the symmetry of the displacement field of figures 2(d) and S2(c) shows that the Curie principle of symmetry is fulfilled. The unique initial symmetry element (the vertical dashed line at $i = \frac{N_{\mathrm{x}}}{2}$) is preserved after the substrate-membrane deformation. Indeed, the line $i = \frac{N_{\mathrm{x}}}{2}$ is the plane of symmetry of the displacement field. Along the latter line all vectors are equal to zero.

Table 2. Number of nn and nnn bonds in the membrane, substrate, and interface.

Number of bonds	Membrane	Substrate	Interface
nn bonds	$(N_m-2)\,(2N_x-1)$	$N_s(2N_x-1)$	(N_x-1)
nnn bonds	$2(N_x-1)(N_m-2)$	$2(N_x-1)(N_s-2)$	$2(N_x-1)$

Table 3. Low-spin instantaneous and equilibrium nn and nnn distances in the membrane, substrate, and interface, considered in the analytical elastic energy of equation (8).

Bond lengths	nn distance	nnn distance	nn equilibrium distance	nnn equilibrium distance
LS membrane	x	$x\cdot\sqrt{2}$	R_0^{LL}	$R_0^{LL}\sqrt{2}$
Substrate	x	$x\cdot\sqrt{2}$	R_{sub}	$R_{sub}\sqrt{2}$
Interface	x	$x\cdot\sqrt{2}$	$\frac{(R_0^{LL}+R_{sub})}{2}$	$\frac{R_0^{LL}+R_{sub}}{2}\sqrt{2}$

3.2. Analytical expressions of the relaxed lattice parameters

To check the general consistency of the present MC results, the elastic properties of the system were inspected analytically. It is worth mentioning that the interplay between the elastic properties of the membrane and the substrate is a complex problem, whose an exact analytical treatment is out of reach.

Here, we develop an approximate method to evaluate the analytical expressions of the relaxed lattice parameters. The basic idea is to treat the lattice uniformly, by setting all instantaneous nn distances equal to x. First, we summarize in table 2 the expressions of the number of nn and nnn bonds inside the membrane, the interface and the substrate, as a function of N_m, N_s and N_x. On the other hand, the total number of sites in the system is, $N_x\cdot(N_m+N_s)$, while inside the membrane and the substrate they are respectively, equal to $N_x\cdot N_m$ and $N_x\cdot N_s$.

For an LS membrane, the equilibrium distance between nn membrane (resp. nnn) sites is equal to R_0^{LL} (resp. $R_0^{LL}\sqrt{2}$), while that of the substrate is R_{sub} (resp $\cdot\, R_{sub}\sqrt{2}$) and that of a site located at the interface is $\frac{R_{sub}+R_0^{LL}}{2}$ (resp. $\frac{R_{sub}+R_0^{LL}}{2}.\ \sqrt{2}\Big)$. The instantaneous nn (resp. nnn) distances assumed here as uniform over the lattice are denoted x (resp. $x\sqrt{2}$). All these information, about the instantaneous and equilibrium bond lengths distances, are summarized in table 3.

Following earlier analytical methods developed in [89, 99] and using the data of tables 2 and 3, we can calculate the total elastic energy, as:

$$E_{elas}(x) = a\cdot(x-R_{LS})^2 + b\cdot(x-R_{int})^2 + c\cdot(x-R_{sub})^2 \tag{8}$$

where the expressions of a, b, c denote the effective elastic constant. The latter parameters are connected to the elastic constants A and B as expressed in equations S1–S3 of the SI. We should state that the anharmonic effects was neglected in this analytical study.

Minimizing E_{elas} with respect to x gives access, analytically, to the relaxed lattice parameter x_{relax}:

$$x_{relax} = \alpha_{LS}R_{LS} + \beta_{LS}R_{sub} + \gamma_{LS}R_{int} \tag{9}$$

$$\text{with,}\quad \alpha_{LS} = \frac{a}{a+b+c},\quad \beta_{LS} = \frac{c}{a+b+c}\quad \text{and}\quad \gamma_{LS} = \frac{b}{a+b+c}$$

The dependence of the average lattice parameter with that of the substrate is presented in insert of figure 2(c) for the MC and analytical calculations. An excellent agreement was found confirming, thus, the relevance of the present analytical methods.

3.3. Thermo-induced spin transition

Now we analyze the effect of the equilibrium lattice parameter of the substrate on the thermo-induced spin transition of the relaxed membrane. The temperature is varied from 0 to 300 K on heating and cooling with a thermal step of 1 K. The thermo-induced spin transitions for the different substrate's lattice parameters, R_{sub}, are illustrated in figures 3(a) and (b) in terms of n_{HS} and membrane's lattice parameter, respectively.

Figure 3(c) indicates the presence of a non-monotonous evolution of the thermal hysteresis width, ΔT, as a function of R_{sub}. The maximum value of ΔT (≈ 75 K) was obtained for a substrate bond length $R_{sub} = 1.1$nm. In fact, the latter value of R_{sub} is equal to $R_0^{HL} = \frac{R_0^{LL}+R_0^{HH}}{2}$, which corresponds to the best elastic coupling between the HS and LS sublattices. A substrate whose $R_{sub} \leqslant \frac{R_0^{HH}+R_0^{LL}}{2} = 1.1$ nm generates a compressive strain that promotes the LS state, and thus shifts the equilibrium temperature, $T_{eq} = \frac{T_{HS\to LS}+T_{LS\to HS}}{2}$, toward higher values $\sim$170 K. (Here, $T_{HS\to LS}$ and $T_{LS\to HS}$ are the transition temperatures from HS to LS and LS to HS, respectively.) Whereas, the substrate, whose $R_{sub} \geqslant 1.2$nm, applies an important tensile strain on the SCO membrane that considerably decreases the transition temperature (~ 90 K), and enhances the 1st order character of the transition. We should

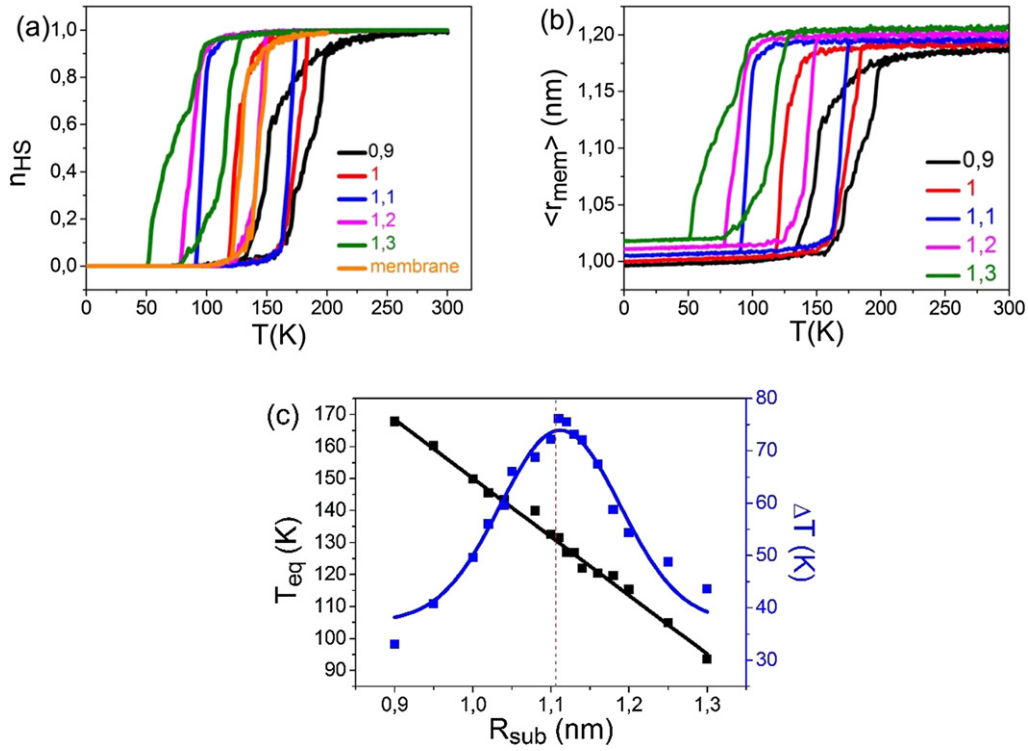

Figure 3. Thermal dependence of the HS fraction, n_{HS} (a) and average membrane bond lengths, $\langle r_{mem} \rangle$, (b) for different substrate's lattice parameters. (c) The evolution of the equilibrium temperature T_{eq} (black squares) and the hysteresis width ΔT (blue squares) as a function of the substrate's lattice parameter.

mention that the presence of the substrate leads to an increase of the hysteresis width ΔT (> 40K) as it was equal to ~ 14K for an isolated membrane.

Figure 3(a) shows that for $R_{sub} = 0.9$ (resp. $R_{sub} = 1.3$) the thermal hysteresis has a two-step transition, with a pinched region around the LS (resp. HS) state and an asymmetric shape. The two-step feature will explained on the basis of the nucleation and propagation of the spin states in the membrane. The small lattice parameter of the membrane, for example $R_{sub} = 0.9$nm (see black curves in figure 3(a) and (b)), drives the change of the HS fraction on cooling progressively well before the advent of the sharp transition at $\sim$150 K. On heating, the transition proceeds in a non-symmetric way following a two-step behavior. Very similar trends are also obtained for $R_{sub} = 1.3$, where the gradual part appears on heating and the marked two-step transition happens on cooling (red curves of figure 3(a) and (b)).

We should stress here on the fact that the total local effective ligand field acting on an SCO site, in the frame of this electro-elastic model, contains an elastic field contribution originating from the surrounding environment (neighboring sites, surface atoms, interface etc) [24, 70, 72]. Thus, one may easily imagine that the SCO sites close to the substrate interface might have a different ligand field compared to those located inside the membrane or in the surface.

Beyond the present structural properties of the substrate, it was reported in the literature that charge transfers at the interface [50] as well as adsorption configurations [51] may also significantly influence the local ligand field and then affecting the spin transition temperatures and strength of the interactions.

3.4. Structural properties

To explain the structural synergy between the substrate and the membrane, we plotted the lattice parameters along the thermo-induced spin transition in figures 3(b), S2(a) and (b), for different values of R_{sub}. Interestingly, figure 3(b) reveals the presence of a tensile strain (resp. compressive) in the LS state for $R_{sub} > R_0^{HL}$ (resp. $R_{sub} < R_0^{HL}$) which slightly affects n_{HS} at low temperatures (see figure 3(a)). In addition, figure S2(b) in SI, clearly shows that the average bond lengths are slightly disturbed through the thermal loop.

Furthermore, at higher temperatures, corresponding to the HS state of the SCO membrane, the lattice parameters (membrane and substrate) show a linear relationship as a function of R_{sub}, as reported in figure S2(c) of SI. The lattice parameter of the LS membrane is less sensitive to the structural misfit between the substrate and the membrane than that of HS state, where in the latter case the slope of $\langle r_{mem} \rangle$ vs R_{sub} was estimated around 0.4 compared to 0.2 in the LS state. Similarly, we used the data of table 3 and calculated analytically the total elastic energy in the homogenous case. After mechanical relaxation, the obtained values of $x_{relax}(R_{sub})$ were in excellent agreement with MC data (figure S2(d)).

3.5. Spatiotemporal aspects of the HS/LS nucleation

We have as well analyzed the effect of the substrate's lattice parameter on the spatio-temporal aspects of the

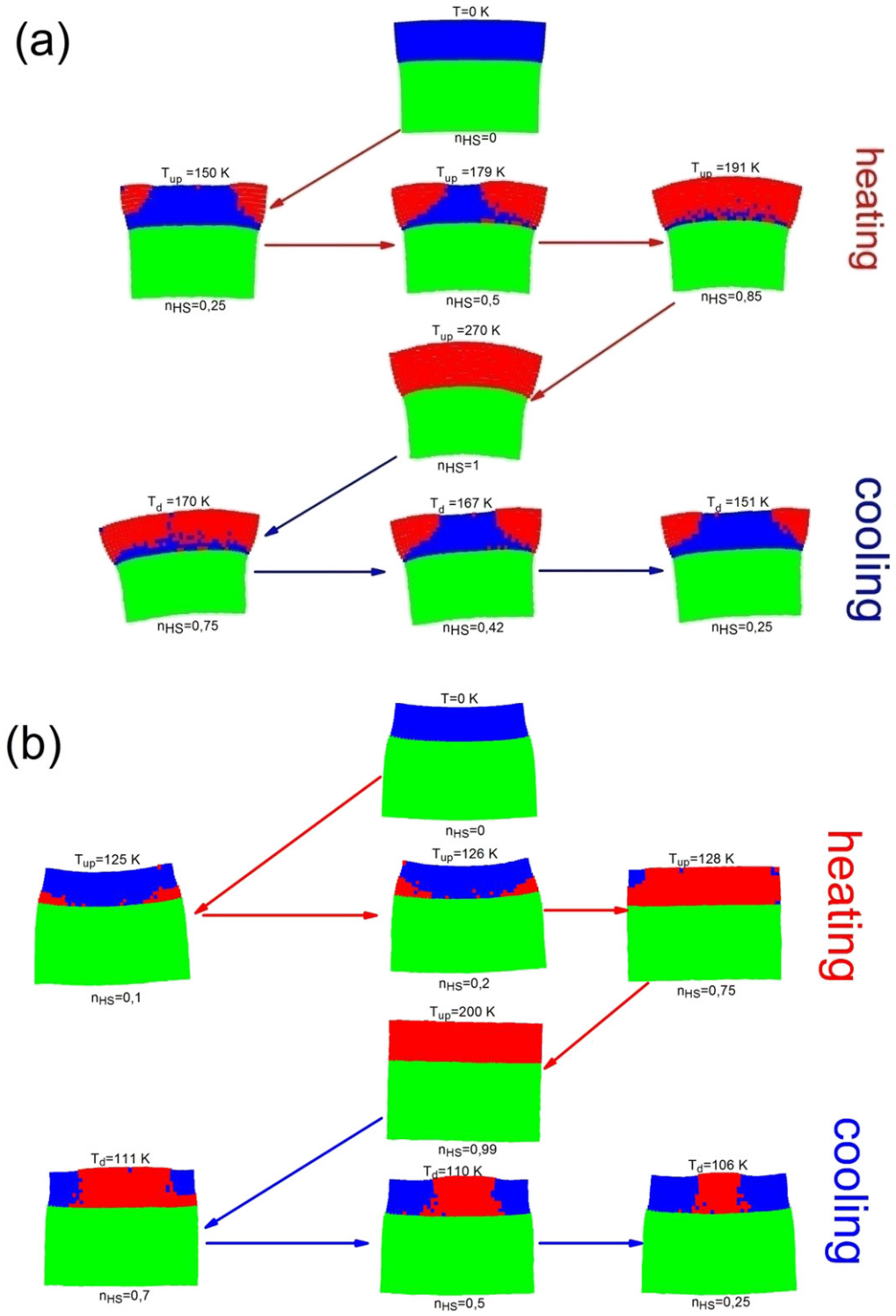

Figure 4. Snapshots of the system (membrane + substrate) during the heating and the cooling process for (a) $R_{\text{sub}} = 0.9$ nm and (b) $R_{\text{sub}} = 1.2$ nm. The red (blue) dots denote HS (LS) sites and the green dots correspond to the substrate atoms.

thermo-induced spin transition. The snapshots of the spin state configuration and the lattice deformation along the thermal hysteresis loop are summarized in figures 4(a) and (b) for $R_{\text{sub}} = 0.9$ and 1.2 nm, respectively. Figure 4(a) reveals that upon heating process ($n_{\text{HS}} = 0.25$), the HS phase grows exclusively and quite easily (due to surface effects) from the free corners. Then, the HS phase spreads over the entire membrane by an anisotropic way along the edges and avoiding the interface between the membrane and the substrate. The interface converts only at the end of the process, due to the lower value of the lattice bond length in this region. The latter behavior explains the particular shape of the thermal hysteresis of figure 3(a) on heating, which shows a rapid growth of the HS fraction followed by a slow process due to

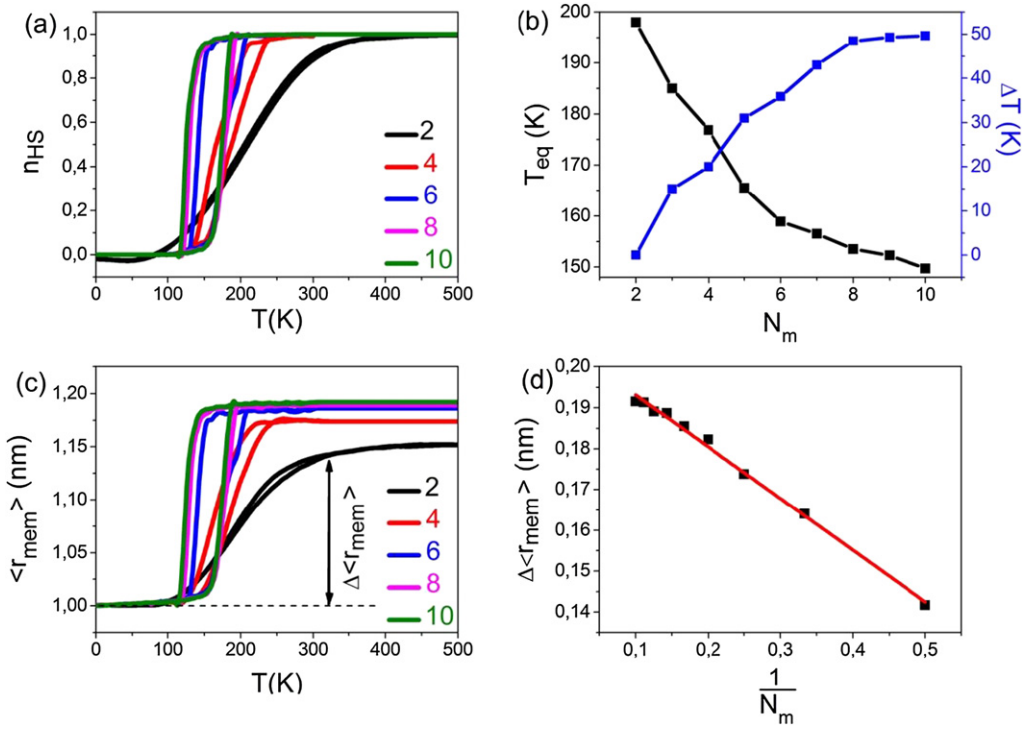

Figure 5. (a) Thermal dependence of n_{HS} as a function of the membrane's thickness N_{m}. (b) Variation of T_{eq} (black square) and ΔT (blue square) as a function of the thickness of the membrane N_{m}. (c) Thermal dependence of $\langle r_{\mathrm{mem}} \rangle$ as a function of the thickness N_{m}. (d) Variation of $\Delta \langle r_{\mathrm{mem}} \rangle = \langle r_{\mathrm{mem}}^{\mathrm{HS}} \rangle - \langle r_{\mathrm{mem}}^{\mathrm{LS}} \rangle$ as a function of $\frac{1}{N_{\mathrm{m}}}$. The elastic constants of the membrane and the substrate were fixed to $A_{\mathrm{mem}} = A_{\mathrm{sub}} = 30\,000\,\mathrm{K\,nm^{-2}}$.

the influence of the substrate. Indeed, the compressive stress exerted by the substrate (whose lattice parameter is smaller than that of LS state) on the membrane atoms localized in the vicinity of the membrane/substrate interface delays the thermal switching. In contrast, the spatio-temporal aspects of the HS $\rightarrow$ LS transition on cooling, for $R_{\mathrm{sub}} = 0.9\,\mathrm{nm}$, are completely different from those observed on heating. Due to the reduced lattice value around the interface, the nucleation of the LS phase starts preferentially around the interface region (see figure 4(a)), propagates first longitudinally toward the center and then transversally along the corners.

On the other hand, for $R_{\mathrm{sub}} = 1.2\,\mathrm{nm}$, the processes of nucleation and growth are almost opposite to those of $R_{\mathrm{sub}} = 0.9$. Indeed, on heating the nucleation of HS species starts around LS sites located at the surface, in the vicinity of the membrane/substrate interface (figure 4(b)), where the sites in question experience a tensile stress. The HS phase propagates transversally along the interface line and then longitudinally along the center, where the corners are the last to switch. On cooling the LS phase grows from the free corners and top surface and propagates toward the center of the membrane. The atoms of the membrane in the vicinity of the substrate have longer relaxation times because they are stabilized by the tensile stress induced by the substrate.

3.6. Effects of the membrane thickness

In figure 5(a), we plotted the thermal variation of the HS fraction for various membrane thicknesses, N_{m}, at a fixed substrate thickness, N_{s}. Initially at 0 K, we construct the system with uniform bond lengths equal to those of the LS membrane, i.e. $R_{\mathrm{sub}} = R_{\mathrm{mem}} = R_0^{\mathrm{LL}}$. As expected, the results show that the abrupt transition character is enhanced when we increase the thickness of the membrane, while for thin membranes, gradual spin transitions are obtained. In addition, thicker membranes lead to a significant shift of the thermal hysteresis loop and thus the transition temperature T_{eq} shifts toward low temperatures. The shift is estimated around 50 K between the thickest ($N_{\mathrm{m}} = 10$) and the thinnest membrane ($N_{\mathrm{m}} = 2$). In contrast, the hysteresis width increases with N_{m} (figure 5(b)) simply due to the size increase of the membrane in usual 2D SCO simulations.

Furthermore, to understand the mechanical effects between the membrane and the substrate, we followed the thermal variation of their average nn distances, depicted in figure 5(c). We easily notice a slight difference in the shape of the hysteresis loops of n_{HS} and lattice parameters, especially in the high temperature region, where the nn distance of the membrane hardly reaches the equilibrium HS distance for thin membranes. As a result, a linear dependence is obtained between $\Delta \langle r_{\mathrm{mem}} \rangle = \langle r_{\mathrm{mem}}^{\mathrm{HS}} \rangle - \langle r_{\mathrm{mem}}^{\mathrm{LS}} \rangle$ and the inverse of membrane's thickness $\frac{1}{N_{\mathrm{m}}}$ (figure 5(d)).

4. Conclusion

In conclusion, we have investigated the thermo-induced spin transition of an SCO membrane deposited on a substrate through an electro-elastic model. We have seen that this configuration allows an efficient mechanical coupling between

the two materials since they influence the thermodynamic of each other. Due to this mechanical coupling, the thermal properties of the SCO membrane agree with the structural and mechanical features of the membrane. Our major finding is in a good agreement with the experimental observations and the anterior reports [52]. Such analysis clearly shows the crucial influence of the substrate's lattice parameter on the thermal, mechanical and structural properties of the SCO membrane. These results showed that the increase of R_{sub} leads to a shift of the whole hysteresis loop toward lower temperatures with a non-monotonous variation of the hysteresis width. Particularly, by adjusting R_{sub}, we were able to control the cooperativity, the thermal properties, and even its mechanical properties. For a lattice parameter ($R_{sub} = 0.9$ nm), the spatial distribution of the HS fraction takes place through the corner of membrane, whereas for ($R_{sub} = 1.2$ nm), the HS fraction takes place through the interface membrane substrate as they have the same lattice parameter ($R_0^{HS} = R_{sub}$). We explained the latter effect through the appearance of a negative pressure on the interface between the membrane and the substrate. In fact, for a ($R_{sub} < 1$ nm), we demonstrated the presence of a positive (resp. negative) pressure (or elastic energy) inside the membrane (resp. in the substrate) that hinders the volume expansion. However, for ($R_{sub} > 1$ nm), the pressure becomes negative in the membrane and positive in the substrate. We showed that the pressure is mainly localized around the interface so as it highly impacted the spatiotemporal aspects of the spin transition.

Such behaviors underline the crucial role of the substrate in the magnetic and mechanical properties of the membrane; our results are in good agreement with the experimental ones reported in reference [52], where the authors observed a restoration of the hysteresis loop due to an important cooperativity when Fe(pyrazine) $Pt(CN)_4$ is coated with a thin film silica, unlike softer substrate which destroys the cooperativity. It is interesting to mention that the reasoning developed here is based on the effect of 'elastic strain engineering'. The latter effect could be used for several applications such as to control the photo-magnetic properties of nanostructures of Prussian blue analogs [24], and more globally to tailor the properties of graphene [100, 101] as well as to enhance the properties of known ferroic oxides or to create new tunable microwave dielectrics [102–104]. Here, we demonstrated that the lattice mismatch between the substrate and the membrane may serve as a powerful tool to control and adjust the magnetic and structural properties of the SCO thin films in order to achieve or to create or enhance new emerging properties.

Acknowledgments

The authors acknowledge the support received from CNRS (Center National de la Recherche Scientifique), the University of Versailles, University Paris-Saclay and Tunisian Ministry of Higher Education and Scientific Research.

ORCID iDs

A Slimani https://orcid.org/0000-0002-4303-4169

References

[1] König E 1991 *Nature and Dynamics of the Spin-State Interconversion in Metal Complexes* (Berlin: Springer) pp 51–152
[2] Linares J, Codjovi E and Garcia Y 2012 Pressure and temperature spin crossover sensors with optical detection *Sensors* **12** 4479
[3] Molnar G, Niel V, Real J A, Dubrovinsky L, Bousseksou A and Mc-Garvey J 2003 Raman spectroscopic study of pressure effects on the spin-crossover coordination polymers Fe(pyrazine)$[M(CN)_4] \cdot 2H_2O$ (M = Ni, Pd, Pt). First observation of a piezo-hysteresis loop at room temperature *J. Phys. Chem.* B **107** 3149
[4] Gutlich P 1981 *Struct. Bond.* **44** 83
[5] Bousseksou A, Boukheddaden K, Goiran M, Consejo C, Boillot M L and Tuchagues J P 2002 Dynamic response of the spin-crossover solid $Co(H_2(fsa)_2en)(py)_2$ to a pulsed magnetic field *Phys. Rev.* B **65** 172412
[6] Prins F, Monrabal-Capilla M, Osorio E A, Coronado E and van der Zant H S J 2011 Room-temperature electrical addressing of a bistable spin-crossover molecular system *Adv. Mater.* **23** 1545
[7] Nishi K, Arata S, Matsumoto N, Iijima S, Sunatsuki Y, Ishida H and Kojima M 2010 One-dimensional spin-crossover iron(II) complexes bridged by intermolecular imidazole-pyridine NH···N hydrogen bonds, [Fe(HLMe)3]X2 (HLMe = (2-methylimidazol-4-yl-methylideneamino-2-ethylpyridine; X = PF_6, ClO_4, BF_4) *Inorg. Chem.* **49** 1517–23
[8] Koike M, Murakami K, Fujinami T, Nishi K, Matsumoto N and Sunatsuki Y 2013 Syntheses, three types of hydrogen-bonded assembly structures, and magnetic properties of [FeIII(Him)$_2$(hapen)]Y · solvent (Him = imidazole, hapen = N,N′−bis (2−hydroxyacetophenylidene) ethylenediamine, Y = BPh_4^-, $CF_3SO_3^-$, PF_6^-, ClO_4^-, and BF_4^- *Inorg. Chim. Acta* **399** 185–92
[9] Gutlich P, Hausser A and Spiering H 1994 Thermal and optical switching of iron(II) complexes *Angew. Chem., Int. Ed. Engl.* **33** 2024
[10] Gallois B, Real J A, Hauw C and Zarembowitch J 1990 Structural changes associated with the spin transition in bis (isothiocyanato) bis (1,10−phenanthroline)iron: a single-crystal x-ray investigation iron: a single-crystal x-ray investigation *Inorg. Chem.* **29** 1152
[11] Willenbacher N and Spiering H 1988 The elastic interaction of high-spin and low-spin complex molecules in spin-crossover compounds *J. Phys. C: Solid State Phys.* **21** 1423–39
[12] Boukheddaden K 2013 Monte Carlo investigations on surface elastic energy of spin-crossover solids: direct access to image pressure and the Eshelby constant *Phys. Rev.* B **88** 134105
[13] Spiering H, Meissner E, Köppen H, Müller E W and Gütlich P 1982 The effect of the lattice expansion on high spin ⇌ low spin transitions *Chem. Phys.* **68** 65–71
[14] Ohnishi S and Sugano S 1981 Strain interaction effects on the high-spin-low-spin transition of transition-metal compounds *J. Phys. C: Solid State Phys.* **14** 39–55
[15] Decurtins S, Gutlich P, Kohler C P, Spiering H and Hauser A 1984 Light-induced excited spin state trapping in a transition-metal complex: the hexa-1-propyltetrazole-iron (II) tetrafluoroborate spin-crossover system *Chem. Phys. Lett.* **105** 1
[16] Muller E W, Ensling J, Spiering H and Gutlich P 1983 High-spin .dblharw. low-spin transition in hexacoordinate complexes of iron(II) with monodentate 1-alkyltetrazole ligands: a variable-temperature Mossbauer, magnetic susceptibility, and far-infrared study *Inorg. Chem.* **22** 2074
[17] Vos G, Le Fèbre R A, de Graff R A G, Haasnoot J G and Reedijk J 1983 Unique high-spin-low-spin transition of the central

ion in a linear, trinuclear iron (II) triazole compound *J. Am. Chem. Soc.* **105** 1682

[18] Decurtins S, Gutlich P, Hasselbach K M, Hauser A and Spiering H 1985 Light-induced excited-spin-state trapping in iron (II) spin-crossover systems *Inorg. Chem.* **24** 2174–8

[19] Tanaka D, Aketa N, Tanaka H, Tamaki T, Inose T, Akai T, Toyama H, Sakata O, Tajiri H and Ogawa T 2014 Thin films of spin-crossover coordination polymers with large thermal hysteresis loops prepared by nanoparticle spin coating *Chem. Commun.* **50** 10074

[20] Forestier T, Mornet S, Daro N, Nishihara T, Mouri S, Tanaka K, Fouche O, Freysz E and Létard J-F 2008 Nanoparticles of iron(II) spin-crossover *Chem.Commun.* 4327

[21] Forestier T, Kaiba A, Pechev S, Denux D, Guionneau P, Etrillard C, Daro N, Freysz E and Létard J-F 2009 Nanoparticles of $[Fe(NH_2-trz)_3]Br_2\cdot 3H_2O$ $(NH_2-trz=2-amino-1,2,4-triazole)$ prepared by the reverse Micelle technique: influence of particle and coherent domain sizes on spin-crossover properties *Chem. Eur. J.* **15** 6122

[22] Coronado E, Galán-Mascarós J R, Monrabal-Capilla M, García-Martínez J and Pardo-Ibáñez P 2007 Bistable spin-crossover nanoparticles showing magnetic thermal hysteresis near room temperature *Adv. Mater.* **19** 1359

[23] Felts A C, Andrus M J, Knowles E S, Quintero P A, Ahir A R, Risset O N, Li C H, Maurin I, Halder G J, Abboud K A, Meisel M W and Talham D R 2016 Evidence for interface induced strain and its influence on photo magnetism in Prussian blue analogue core–shell heterostructures $Rb_aCo_b[Fe(CN)_6]_c.mH_20@K_jNi_k[Cr(CN)_6]_l.nH_2O$ *J. Phys. Chem.* C **120** 5420

[24] Felts A C, Slimani A, Cain J M, Andrus M J, Ahir A R, Abboud K A, Meisel M W, Boukheddaden K and Talham D R 2018 Control of the speed of a light-induced spin transition through mesoscale core–shell architecture *J. Am. Chem. Soc.* **140** 5814–24

[25] Tissot A, Enachescu C and Boillot M L 2012 Control of the thermal hysteresis of the prototypal spin-transition $Fe^{II}(phen)_2(NCS)_2$ compound via the microcrystallites environment: experiments and mechanoelastic model *J. Mater. Chem.* **22** 20451

[26] Chen Y, Ma J-G, Zhang J-J, Shi W, Cheng P, Liao D-Z and Yan S-P 2010 Spin crossover-macromolecule composite nano film material *Chem. Commun.* **46** 5073

[27] Lee S-W, Lee J-W, Jeong S-H, Park I-W, Kim Y-M and Jin J-I 2004 Processable magnetic plastics composites—spin crossover of PMMA/Fe(II)-complexes composites *Synth. Met.* **142** 243

[28] Martinez V, Boldog I, Gaspar A B, Ksenofontov V, Bhattacharjee A, Gütlich P and Real J A 2010 Spin crossover phenomenon in nanocrystals and nanoparticles of $\left[Fe(3-Fpy)_2M(CN)_4\right]$ $\left(M^{II}=Ni,Pd,Pt\right)$ two-dimensional coordination polymers *Chem. Mater.* **22** 4271

[29] Rubio M, Hernández R, Nogales A, Roig A and López D 2011 Structure of a spin-crossover Fe(II)—1,2,4-triazole polymer complex dispersed in an isotactic polystyrene matrix *Eur. Polym. J.* **47** 52

[30] Larionova J, Salmon L, Guari Y, Tokarev A, Molvinger K, Molnar G and Bousseksou A 2008 Towards the ultimate size limit of the memory effect in spin-crossover solids *Angew. Chem., Int. Ed.* **47** 8236

[31] Durand P, Pillet S, Bendeif E E, Carteret C, Bouazaoui M, El Hamzaoui H, Capoen B, Salmon L, Hebert S, Ghanbaja J, Aranda L and Schaniel D 2013 Room temperature bistability with wide thermal hysteresis in a spin crossover silica nanocomposite *J. Mater. Chem.* C **1** 1933

[32] Tissot A, Bardeau J-F, Rivière E, Brisset F and Boillot M-L 2010 Thermo- and photo switchable spin-crossover nanoparticles of an iron(II) complex trapped in transparent silica thin films *Dalton Trans.* **39** 7806

[33] Titos-Padilla S, Herrera J M, Chen X-W, Delgado J J and Colacio E 2011 Bifunctional hybrid SiO2 nanoparticles showing synergy between core spin crossover and shell luminescence properties *Angew. Chem., Int. Ed. Engl.* **50** 3290

[34] Faulmann C, Chahine J, Malfant I, de Caro D, Cormary B and Valade L 2011 A facile route for the preparation of nanoparticles of the spin-crossover complex $[Fe(Htrz)_2(trz)](BF_4)$ in xerogel transparent composite films *Dalton Trans.* **40** 2480

[35] Adam A, Poggi M, Larquet E, Cortès R, Martinelli L, ECoulon P, Lahera E, Proux O, Chernyshov D, Boukheddaden K, Gacoin T and Maurin I 2018 Strain engineering of photo-induced phase transformations in Prussian blue analogue heterostructures *Nanoscale* **10** 16030

[36] Fourati H, Milin E, Slimani A, Chastanet G, Abid Y, Triki S and Boukheddaden K 2018 Interplay between a crystal's shape and spatiotemporal dynamics in a spin transition material *Phys. Chem. Chem. Phys.* **20** 10142–54

[37] P-Espejo M, Sy M and Boukheddaden K 2018 Unprecedented bistability in spin-crossover solids based on the retroaction of the high spin low-spin interface with the crystal bending *J. Am. Chem. Soc.* **140** 11954–64

[38] Sy M, Garrot D, Slimani A, Paez-Espejo M, Varret F and Boukheddaden K 2016 Reversible control by light of the high-spin low-spin elastic interface inside the bistable region of a robust spin transition single crystal *Angew. Chem., Int. Ed. Engl.* **55** 1755–9

[39] Sorai M, Yumoto Y, Dost M H and Larkworthy L F 1993 Calorimetric study on the spin-crossover phenomenon between 3T1 and 5E in trans-bis[1,2-bis(diethylphosphino) ethane] diiodochromium(II), $[CrI_2(depe)_2]$ *J. Phys. Chem. Solids* **54** 421–30

[40] Lefter C, Davesne V, Salmon L, Molnar G, Demont P, Rotaru A and Bousseksou A 2016 Charge transport and electrical properties of spin crossover materials: towards nanoelectronic and spintronic devices *Magnetochemistry* **2** 18

[41] Lefter C, Rat S, Costa J S, Manrique-Juarez M D, Quintero C M, Salmon L, Séguy I, Leichle T, Nicu L, Demont P, Rotaru A, Molnar G and Bousseksou A 2016 Current switching coupled to molecular spin-states in large-area junctions *Adv. Mater.* **28** 7508

[42] Dugay J, Giménez-Marqués M, Kozlova T, Zandbergen H W, Coronado E and van der Zant H S J 2015 Spin switching in electronic devices based on 2D assemblies of spin-crossover nanoparticles *Adv. Mater.* **27** 1288

[43] Holovchenko A, Dugay J, Giménez-Marqués M, Torres-Cavanillas R, Coronado E and van der Zant H S J 2016 Near room-temperature memory devices based on hybrid spin-crossover@SiO_2 nanoparticles coupled to single-layer graphene nanoelectrodes *Adv. Mater.* **28** 7228

[44] Benaicha B, Van Do K, Yangui A, Pittala N, Lusson A, Sy M, Bouchez G, Fourati H, Gomez-Garcia C J, Triki S and Boukheddaden K 2019 Interplay between spin-crossover and luminescence in a multifunctional single crystal iron(II) complex: towards a new generation of molecular sensors *Chem. Sci.* **10** 6791–8

[45] Boukheddaden K, Ritti M H, Bouchez G, Sy M, Dîrtu M M, Parlier M, Linares J and Garcia Y 2018 Quantitative contact pressure sensor based on spin crossover mechanism for civil security applications *J. Phys. Chem.* C **122** 7597–604

[46] Naik A D, Robeyns K, Meunier C F, Léonard A F, Rotaru A, Tinant B, Filinchuk Y, Su B L and Garcia Y 2014 Selective and reusable iron(II)-based molecular sensor for the vapor-phase detection of alcohols *Inorg. Chem.* **53** 1263–5

[47] Matsuda M, Isozaki H and Tajima H 2008 Reproducible on-off switching of the light emission from the electroluminescent device containing a spin crossover complex *Thin Solid Films* **517** 1465

[48] Abdul-Kader K, Lopes M, B-Murgui C, Kraieva O, Lionel Salmon E M H, Nicolazzi W, Carcenac F, Thibault C, Molnár G and Bousseksou A 2013 Synergistic switching of plasmonic resonances and molecular spin states *Nanoscale* **5** 5288–93

[49] Gaita-Ariño A, Luis F, Hill S and Coronado E 2019 Molecular spins for quantum computation *Nat. Chem.* **11** 301–9

[50] Zhang Y 2015 Mingsen Deng electrical control of spin states of ferrocene on Cu(111) *J. Phys. Chem.* C **119** 21681–7

[51] Zhang Y 2018 Driving spin transition at interface: role of adsorption configurations *J. Chem. Phys.* **148** 044706

[52] Raza Y, Volatron F, Moldovan S, Ersen O, Huc V, Martini C, Brisset F, Gloter A, Stéphan O, Bousseksou A, Catala L and Mallah T 2011 Matrix-dependent cooperativity in spin crossover Fe(pyrazine)$Pt(CN)_4$nanoparticles *Chem. Commun.* **47** 11501

[53] Kahn O 1993 *Molecular Magnetism* (New York: VCH)

[54] Boukheddaden K, Linares J, Codjovi E, Varret F, Niel V and Real J A 2003 *J. Appl. Phys.* **93** 7103–5

[55] Real J A, Gaspar A B, Muñoz M C, Gütlich P, Ksenofontov V and Spiering H 2004 Spin crossover in transition metal compounds I *Topics in Current Chemistry,* ed P Gütlich and H A Goodwin (Berlin: Springer) vol 233 pp 167–93

[56] Bousseksou A, Nasser J, Linares J, Boukheddaden K and Varret F 1992 Ising-like model for the two-step spin-crossover *J. Phys.* I **2** 1381

[57] Romstedt H, Hauser A and Spiering J 1998 High-spin → low-spin relaxation in the two-step spincrossover compound $[Fe(pic)_3]Cl_2EtOH$ (pic = 2-picolylamine) *Phys. Chem. Solids* **59** 265–75

[58] Törnroos K W, Hostettler M, Chernyshov D, Vangdal B and Bürgi H-B 2006 Interplay of spin conversion and structural phase transformations: re-entrant phase transitions in the 2-propanol solvate of tris(2-picolylamine)iron(II) dichloride *Chemistry* **12** 6207

[59] Gruber M, Davesne V, Bowen M, Boukari S, Beaurepaire E, Wulfhekel W and Miyamachi T 2014 Spin state of spin-crossover complexes: from single molecules to ultrathin films *Phys. Rev.* B **89** 195415

[60] Boukheddaden K, Shteto I, Hôo B and Varret F 2000 Dynamical model for spin-crossover solids. I. Relaxation effects in the mean-field approach *Phys. Rev.* B **62** 14796

[61] Muraoka A, Boukheddaden K, Linares J and Varret F 2011 Two-dimensional Ising-like model with specific edge effects for spin-crossover nanoparticles: a Monte Carlo study *Phys. Rev.* B **84** 054119

[62] Nasser J A 2001 First order high-spin/low-spin phase transition induced by acoustic-phonons *Eur. Phys. J.* B **21** 3–10

[63] Nasser J A, Boukheddaden K and Linares J 2004 Two-step spin conversion and other effects in the atom-phonon coupling model *Eur. Phys. J.* B **39** 219

[64] Stoleriu L, Chakraborty P, Hauser A, Stancu A and Enachescu C 2011 Thermal hysteresis in spin-crossover compounds studied within the mechanoelastic model and its potential application to nanoparticles *Phys. Rev.* B **84** 134102

[65] Miyashita S, Konishi Y, Nishino M, Tokoro H and Rikvold P A 2008 Realization of the mean-field universality class in spin-crossover materials *Phys. Rev.* B **77** 014105

[66] Nishino M, Boukheddaden K, Konishi Y and Miyashita S 2007 Simple two-dimensional model for the elastic origin of cooperativity among spin states of spin-crossover complexes *Phys. Rev. Lett.* **98** 247203

[67] Enachescu C, Stoleriu L, Stancu A and Hauser A 2009 Model for elastic relaxation phenomena in finite 2D hexagonal molecular lattices *Phys. Rev. Lett.* **102** 257204

[68] Nicolazzi W and Pillet S 2012 Structural aspects of the relaxation process in spin crossover solids: phase separation, mapping of lattice strain, and domain wall structure *Phys. Rev.* B **85** 094101

[69] Slimani A, Khemakhem H and Boukheddaden K 2017 Structural synergy in a core-shell spin crossover nanoparticle investigated by an electroelastic model *Phys. Rev.* B **95** 174104

[70] Slimani A, Boukheddaden K, Varret F, Oubouchou H, Nishino M and Miyashita S 2013 Microscopic spin-distortion model for switchable molecular solids: spatiotemporal study of the deformation field and local stress at the thermal spin transition *Phys. Rev.* B **87** 014111

[71] Slimani A, Boukheddaden K and Yamashita K 2015 Effect of intermolecular interactions on the nucleation, growth, and propagation of like-spin domains in spin-crossover materials *Phys. Rev.* B **92** 014111

[72] Oubouchou H, Singh Y and Boukheddaden K 2018 Magnetoelastic modeling of core-shell spin-crossover nanocomposites *Phys. Rev.* B **98** 014106

[73] Slimani A and Boukheddaden K 2018 An electro elastic theory for the mechanically-assisted photo-induced spin transition in core-shell spin crossover nanoparticles *Phys. Chem. Chem. Phys.* **20** 28583–91

[74] Enachescu C and Nicolazzi W 2018 Elastic models, lattice dynamics and finite size effects in molecular spin crossover systems *C. R. Chim.* **21** 1179–95

[75] Stoleriu L, Stancu A, Chakraborty P, Hauser A and Enachescu C 2015 Analysis of first order reversal curves in the thermal hysteresis of spin-crossover nanoparticles within the mechano-elastic model *J. Appl. Phys.* **117** 17B307

[76] Félix G, Nicolazzi W, Salmon L, Molnár G, Perrier M, Maurin G, Larionova J, Long J, Guari Y and Bousseksou A 2013 Enhanced cooperative interactions at the nanoscale in spin-crossover materials with a first-order phase transition *Phys. Rev. Lett.* **110** 235701

[77] Shepherd H J, Molnar G, Nicolazzi W, Salmon L and Bousseksou A 2013 Spin crossover at the nanometre scale *Eur. J. Inorg. Chem.* **2013** 653

[78] Bousseksou A, Molnar G, Salmon L and Nicolazzi W 2011 Molecular spin crossover phenomenon: recent achievements and prospects *Chem. Soc. Rev.* **40** 3313

[79] Nicolazzi W, Pillet S and Lecomte C 2008 Two-variable anharmonic model for spin-crossover solids: a like-spin domains interpretation *Phys. Rev.* B **78** 174401

[80] Mikolasek M, Nicolazzi W, Terki F, Molnár G and Bousseksou A 2017 Surface transition in spin crossover nanoparticles *Chem. Phys. Lett.* **678** 107

[81] Mikolasek M, Nicolazzi W, Terki F, Molnár G and Bousseksou A 2017 Investigation of surface energies in spin crossover nanomaterials: the role of surface relaxations *Phys. Chem. Chem. Phys.* **19** 12276

[82] Félix G, Nicolazzi W, Mikolasek M, Molnár G and Bousseksou A 2014 Non-extensivity of thermodynamics at the nanoscale in molecular spin crossover materials: a balance between surface and volume *Phys. Chem. Chem. Phys.* **16** 7358

[83] Félix G, Mikolasek M, Molnár G, Nicolazzi W and Bousseksou A 2014 Tuning the spin crossover in nano-objects: from hollow to core-shell particles *Chem. Phys. Lett.* **607** 10

[84] Mikolasek M, Félix G, Molnár G, Terki F, Nicolazzi W and Bousseksou A 2014 Role of surface vibrational properties on cooperative phenomena in spin-crossover nanomaterials *Phys. Rev.* B **90** 075402

[85] Affes K, Slimani A, Maalej A and Boukheddaden K 2019 Electro-elastic modeling of thermal and mechanical properties of a spin crossover core/shell nanoparticle *Chem. Phys. Lett.* **718** 46–53

[86] Slimani A, Boukheddaden K and Yamashita K 2014 Thermal spin transition of circularly shaped nanoparticles in a core-shell structure investigated with an electroelastic model *Phys. Rev.* B **89** 214109

[87] Oubouchou H, Slimani A and Boukheddaden K 2013 Interplay between elastic interactions in a core-shell model for spin crossover nanoparticles *Phys. Rev.* B **87** 104104

[88] Boukheddaden K, Slimani A, Sy M, Varret F, Hassane O and Rachid T 2016 *Physical Properties of 2D Spin-Crossover Solids from an Electro-Elastic Description: Effect of Shape, Size, and Spin-Distortion Interactions* (New York: Pan Stanford)

[89] Traiche R, Sy M and Boukheddaden K 2018 Elastic frustration in 1D spin-crossover chains: evidence of multi-step transitions and self-organizations of the spin states *J. Phys. Chem.* C **122** 4083

[90] Enachescu C, Tanasa R, Stancu A, Tissot A, Laisney J and Boillot M-L 2016 Matrix-assisted relaxation in $Fe(phen)_2(NCS)_2$spin-crossover microparticles, experimental and theoretical investigations *Appl. Phys. Lett.* **109** 031908

[91] Jung J, Bruchhäuser F, Feile R, Spiering H and Gütlich P 1996 The cooperative spin transition in $\left[Fe_xZn_{1-x}(ptz)_6\right](BF_4)_2$. I. Elastic properties – an oriented sample rotation study by Brillouin spectroscopy *Z. Phys.* B **100** 517

[92] Spiering H, Boukheddaden K, Linares J and Varret F 2004 Total free energy of a spin-crossover molecular system *Phys. Rev.* B **70** 184106

[93] Sorai M 2004 Heat capacity studies of spin crossover systems *Top. Curr. Chem.* **235** 153

[94] Yu W C and Gielisse P 1971 High pressure polymorphism in CdS, CdSe and CdTe *Mater. Res. Bull.* **6** 621

[95] Nishino M, Enachescu C, Miyashita S, Boukheddaden K and Varret F 2010 Intrinsic effects of the boundary conditions on switching processes in effective long-range interactions originating from local structural change *Phys. Rev.* B **82** 020409(R)

[96] Metropolis N, Rosenbluth A W, Rosenbluth M N, Teller A H and Teller E 1953 *J. Chem. Phys.* **21** 1087

[97] Boukheddaden K and Bailly-Reyre A 2013 Towards the elastic properties of 3D spin-crossover thin films: evidence of buckling effects *Europhys. Lett.* **103** 26005

[98] Stoleriu L, Nishino M, Miyashita S, Stancu A, Hauser A and Enachescu C 2017 Cluster evolution in molecular three-dimensional spin-crossover systems *Phys. Rev.* B **96** 064115

[99] Paez-Espejo M, Sy M and Boukheddaden K 2016 Elastic frustration causing two-step transition in spin-crossover solids: emergence of complex antiferroelastic structures *J. Am. Chem. Soc.* **138** 3202–10

[100] Guinea F, Katsnelson M I and Geim A K 2010 Energy gaps and a zero-field quantum Hall effect in graphene by strain engineering *Nat. Phys.* **6** 30–33

[101] Pereira V M and Castro Neto A H 2009 Strain engineering of graphene's electronic structure *Phys. Rev. Lett.* **103** 046801

[102] Schlom D, Chen L, Fennie C, Gopalan V, Muller D, Pan X and Uecker R 2014 Elastic strain engineering of ferroic oxides *MRS Bull.* **39** 118–30

[103] Setter N and Damjanovic D 2006 Ferroelectric thin films: review of materials, properties, and applications *J. Appl. Phys.* **100** 051606

[104] Chen Y, Lei Y and Li Y *et al* 2020 Strain engineering and epitaxial stabilization of halide perovskites *Nature* **577** 209–15